Phase transitions in defect chalcopyrite compounds under hydrostatic pressure

V. V. Ursaki and I. I. Burlakov
Institute of Applied Physics, Academy of Sciences of Moldova, 2028 Kishinev, Moldova

I. M. Tiginyanu
Technical University of Moldova, 2004 Kishinev, Moldova

Y. S. Raptis and E. Anastassakis
Physics Department, National Technical University, 15780 Athens, Greece

A. Anedda
Dipartimento di Scienze Fisiche, Università di Cagliari, 09124 Cagliari, Italy

(Received 10 March 1998)

Tetrahedrally bonded AGa_2X_4 ($A=$Cd, Zn; $X=$S, Se) compounds crystallizing in defect chalcopyrite and defect famatinite structures have been studied by Raman spectroscopy under hydrostatic pressure. The pressure-induced changes in the Raman spectra of both ordered defect chalcopyrite and partially disordered defect famatinite structures were attributed to an order-disorder phase transition in the cation sublattice, which proved to occur in two stages, as predicted by Bernard and Zunger [Phys. Rev. B **37**, 6835 (1988)]. The first stage of the transition was found to depend on the tetragonal distortion of the initial crystals. An irreversible disappearance of Raman signal at elevated pressures was observed and attributed to a phase transition from the adamantine structure to a high-symmetry rocksalt-type structure. The pressure of this transition in the compounds under consideration exhibits a dependence on bond ionicity and bond length. The structure of decompressed samples was explained on the basis of pressure dependence of potential barriers for the phase transition by using a configuration-coordinate model. [S0163-1829(98)05145-5]

I. INTRODUCTION

Most of ternary adamantine semiconductors with the chemical formula $A^{II}B_2^{III}C_4^{VI}$ crystallizes in the defect chalcopyrite (DC) tetragonal structure. This structure is close to that of chalcopyrite (CP), except that the DC compounds contain a crystallographically ordered array of vacancies (known as stoichiometric voids) in the cation sublattice. The low packing efficiency of constituent atoms in the lattice facilitates the doping of DC compounds by impurities and the formation of solid solutions. DC semiconductors are promising optoelectronic materials due to their high values of nonlinear susceptibility, optical activity, intense luminescence, and high photosensitivity. Some device structures like tunable filters on $CdGa_2S_4$ and UV photodetectors on $CdAl_2S_4$ have already found practical applications.[1,2]

Structural studies of semiconductors present increasing interest in relation to pressure-induced phase transitions, in particular. Numerous studies of II-VI, III-V, and IV-IV compounds have imposed the general understanding of transitions and high-pressure phases, and established structural systematics within each of these systems.[3,4] Phase transitions in $A^{I}B^{III}C_2^{VI}$ chalcopyrite semiconductors have been investigated in considerable detail elsewhere.[5–7] However, only a limited number of high-pressure studies have been performed on defective $A^{II}B_2^{III}C_4^{VI}$ compounds.[8–10] Thus, it has been established that the DC $CdAl_2S_4$ single crystals transform from the adamantine structure to a higher symmetry rocksalt-type structure at pressures ~140 kbar. The Raman spectra were found to undergo substantial changes around 60 and 100 kbar, due to an order-disorder phase transition in the cation sublattice, which occurs in two stages, in accordance with earlier predictions.[11] Further investigations of DC materials under pressure could be of interest for establishing the general systematics of phase transitions in ternary compounds, since $A^{II}B_2^{III}C_4^{VI}$ semiconductors can be obtained in different crystal structures depending on the technological conditions of crystal growth.[12–15]

On the other hand, it is a well-known fact that many semiconductors and their alloys undergo a solid-solid phase transition from disordered structure to an ordered one when the temperature is lowered below a critical value T_c.[16–18] This is related to the fact that different constituent atoms tend to occupy definite sites in the lattice and, as a consequence, long-range order sets in the crystal structure below T_c. This effect has already been studied extensively in tetrahedrally bonded $A^{II}B^{IV}C_2^{V}$ and $A^{I}B^{III}C_2^{VI}$ chalcopyrite compounds.

There are two basic differences between the $A^{I}B^{III}C_2^{VI}$ and $A^{II}B_2^{III}C_4^{VI}$ families. In the former, the valence difference of the disordering cations (A and B) is two, whereas in the latter it is only one and, in addition, there exists an array of vacant sites in the crystal lattice.[19] From this point of view, the disordering process in the DC compounds is energetically more favorable, hence more probable to occur. Some order-disorder effects have been observed in $A^{II}B_2^{III}C_4^{VI}$ compounds with increasing temperature.[20,21] Cation ordering and crystal structures in $A^{II}Ga_2X_4^{VI}$ compounds have been investigated in

 ©1999 The American Physical Society

details elsewhere.[22] A simple relationship was suggested there between the c/a ratio and the cation sublattice ordering.

The goal of this work is to study phase transitions, including order-disorder phenomena, in tetrahedrally bonded $A^{II}Ga_2X_4^{VI}$ compounds with different initial degree of cation disorder, using Raman scattering (RS) spectroscopy under hydrostatic pressure.

II. EXPERIMENT

Single crystals of $A^{II}Ga_2X_4^{VI}$ compounds ($A=$Cd, Zn; $X=$S, Se) were grown by the chemical transport method, the iodine being used as a transport agent.[1] The as-grown samples represent triangular prisms with mirror surfaces. Chemical and structural analyses have proved the stoichiometric composition of the crystals and no spurious phases were observed.

The Raman spectra under pressure were taken in a diamond-anvil cell (DAC) at ambient temperature. No polarized measurements were performed under pressure because of the depolarization of the exciting light by the windows of the pressure chamber. A 4:1 methanol-ethanol mixture was used as a pressure-transmitting medium. The pressure was calibrated to within 0.1 kbar using the ruby luminescence lines. The spectra were measured with a double spectrometer in a nearly backscattering geometry. The 514.5-nm line of an argon laser was used at power level around 30 mW. The laser spot on the sample was 50 μm in diameter and the resolution was better than 1 cm^{-1}.

III. RESULTS

We have undertaken a RS study of $A^{II}Ga_2X_4^{VI}$ compounds ($A=$Cd, Zn; $X=$S, Se) under hydrostatic pressure up to 300 kbar. These compounds are characterized by a variety of structures caused by different degrees of ordering among the cations and vacancies in the cation sublattice. The compounds with $A=$Cd crystallize in the cation-ordered DC tetragonal structure with the space group $I\bar{4}$ (S_4^2, point group S_4).[22–25] While compounds with $A=$Zn crystallize in the defect famatinite (DF) structure having the space group $I\bar{4}2m$ (D_{2d}^{11}, point group D_{2d}) and characterized by partially disordered Zn and Ga cations.[23,26,27] The first-order RS spectrum of the DC structure consists of 13 Raman-active optical modes at the center of the Brillouin zone, namely, $3A+5B+5E$, of which B and E modes are also IR active.[28] The nonpolar A-symmetry modes correspond to oscillations of the anions; the lowest-energy A^1 mode, the so-called ''breathing'' mode, is connected to symmetric oscillations of the anions surrounding a stoichiometric vacancy.[29] The polar B- and E-symmetry modes exhibit LO-TO splitting. The B modes correspond to vibrations of both cations and anions in the z direction, while the E modes correspond to their vibrations in the x-y plane. The Raman-active modes of the DF structure at the center of the zone are $2A_1+2B_1+3B_2+5E$, i.e., one A-symmetry mode less than in the DC structure.[30] In addition, the RS spectra obtained from DF crystals are substantially unpolarized and some peaks are broadened.[27] These effects are caused by the disorder in the cation sublattice.

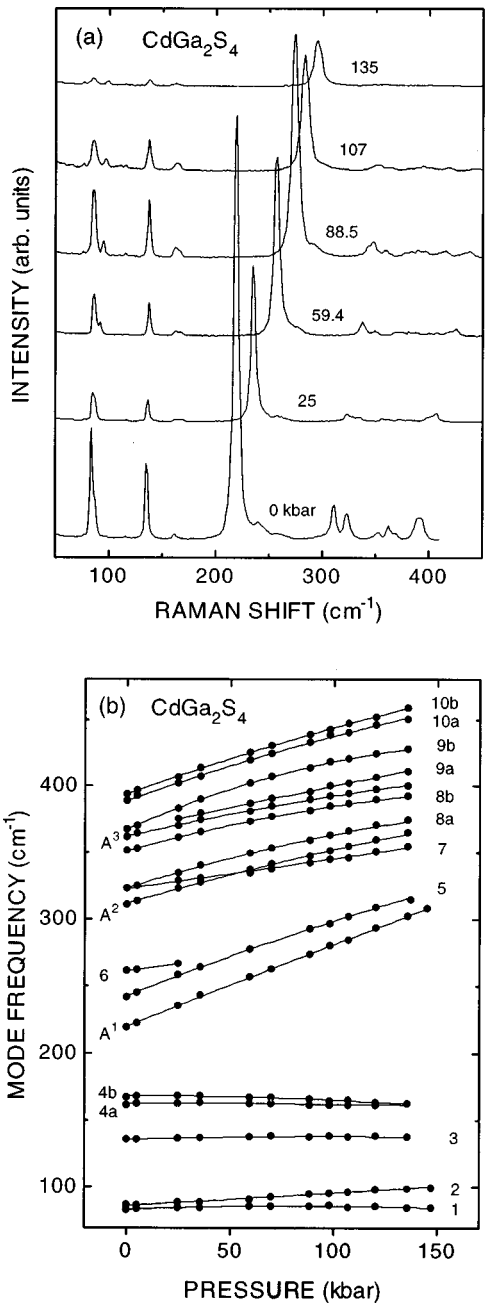

FIG. 1. (a) Raman spectra of $CdGa_2S_4$ at various pressures. (b) Raman shifts vs pressure for the Raman-active modes in $CdGa_2S_4$. Solid lines are quadratic fits. The notations are those of Table I.

Figures 1(a), 2(a), 3(a), and 4(a) show the RS spectra of $CdGa_2S_4$, $CdGa_2Se_4$, $ZnGa_2S_4$, and $ZnGa_2Se_4$, respectively, at various pressures. In order to analyze the pressure behavior of different modes, a spectral deconvolution was used. The mode frequencies were found to increase with pressure increase except for the frequency of the lowest E-symmetry mode. The shifts as a function of pressure are shown in Figs. 1(b), 2(b), 3(b), and 4(b) for $CdGa_2S_4$, $CdGa_2Se_4$, $ZnGa_2S_4$, and $ZnGa_2Se_4$, respectively. Solid lines in the figures represent polynomial fits of the form $\omega=\omega_0+aP+bP^2$ with the frequencies ω and ω_0 in cm^{-1} and P in kbar. The assignment of modes along with the values of ω_0, a, and b are summarized in Table I. The mode assignments are based on earlier RS investigations.[31,32]

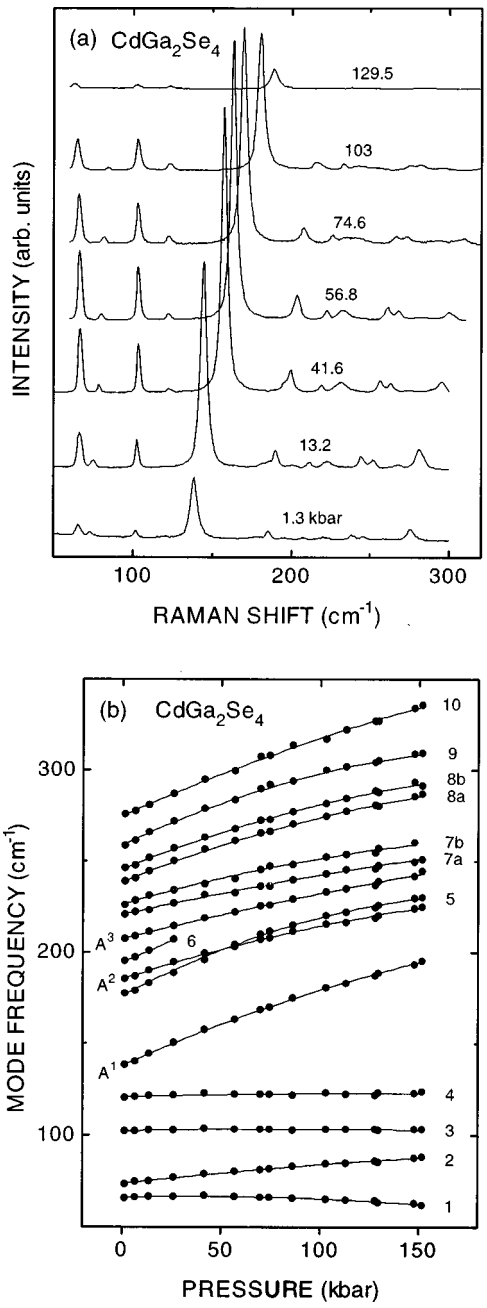

FIG. 2. (a) Same as Fig. 1 for $CdGa_2Se_4$. (b) Same as Fig. 1 for $CdGa_2Se_4$.

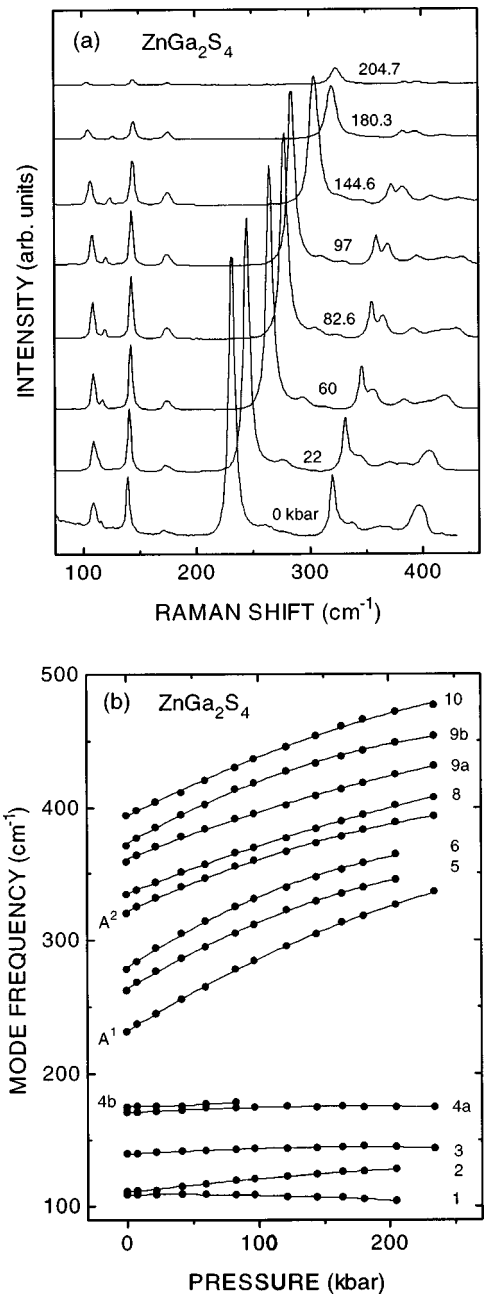

FIG. 3. (a) Same as Fig. 1 for $ZnGa_2S_4$. (b) Same as Fig. 1 for $ZnGa_2S_4$.

The pressure dependence of the RS bands intensity is different for different materials and differs from mode to mode.

Let us first analyze the evolution of the RS spectra for the DC crystals. Figure 5(a) presents the pressure dependence of A^1 mode intensity and the intensity of other modes normalized to that of the A^1 mode in $CdGa_2Se_4$. The intensity of several bands does not exhibit large variations up to pressures around 110 kbar except for a sharp increase at low pressures [see for instance, the mode A^1 in Fig. 5(a)]. The increase of RS intensity at low pressures is caused by the resonance moving away from the laser line with pressure increase. The band gap of $CdGa_2Se_4$ at room temperature and ambient pressure equals 2.57 eV, which is close to the quanta energy of the 514.5-nm laser line. Since dE_g/dP is positive, an increase in band-gap energy with pressure leads to a diminution of the optical absorption coefficient at the wavelength of the laser line. As a result the optical path of the laser beam in the sample and the RS signal increase. At the pressure above 110 kbar the intensity of the modes starts to decrease and the RS signal disappears completely and irreversibly at pressures around 150 kbar [see Fig. 5(a) for A^1 mode]. The rate of the decrease differs from mode to mode. The absolute intensity of the modes near 275 cm^{-1} drops faster than that of the low-frequency modes. The more essential is the sharp decrease of the A^2 mode intensity at pressures above 55 kbar, while the intensity of A^3 and 4 modes begins to increase.

We have also measured the pressure dependence of the full width at half maximum (FWHM) for those modes that exhibit relatively high values of the signal-to-noise ratio. Up

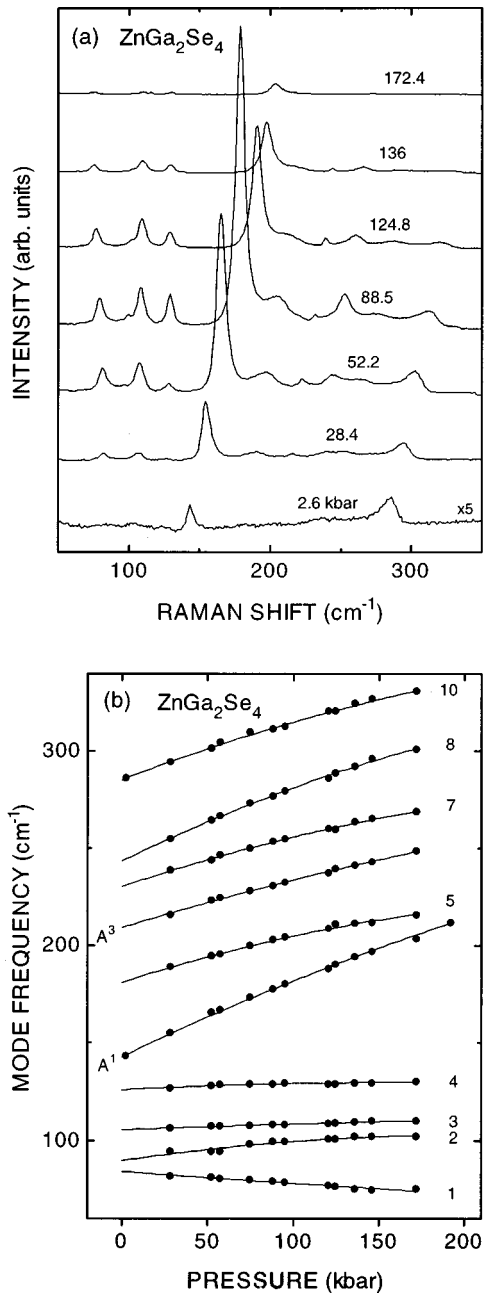

FIG. 4. (a) Same as Fig. 1 for $ZnGa_2Se_4$. (b) Same as Fig. 1 for $ZnGa_2Se_4$.

to 55 kbar, most of the modes exhibit a slight decrease with pressure [if not nearly constant FWHM, as shown in Fig. 5(b)]. At $P>55$ kbar the FWHM for most modes increases with pressure.

An analogous behavior of the RS modes was observed in $CdGa_2S_4$ crystals [see Figs. 6(a) and 6(b)]. The sharp decrease of the A^2 mode intensity in $CdGa_2S_4$ occurs at pressures above 80 kbar [see Fig. 6(a)]. The FWHM of the modes starts to increase at the same pressures around 80 kbar. At pressures above 100 kbar the intensity of the modes begins to decrease and the RS signal disappears completely and irreversibly at pressures around 150 kbar (e.g., A^1 mode).

The behavior of RS modes with pressure in DF crystals exhibits some difference from that of the DC crystals. Figure

TABLE I. Raman-active optical phonon frequencies ω_0 (in cm^{-1}) and their shift parameters a (in 10^{-1} cm^{-1} $kbar^{-1}$) and b (in -10^{-4} cm^{-1} $kbar^{-2}$) for $A^{II}Ga_2X_4^{VI}$ compounds. The longitudinal optical (LO) and transverse optical (TO) mode assignments are from Refs. 31 and 32.

Curve	Mode assignment	$CdGa_2S_4$ ω_0	$CdGa_2S_4$ a	$CdGa_2S_4$ b	$ZnGa_2S_4$ ω_0	$ZnGa_2S_4$ a	$ZnGa_2S_4$ b	$CdGa_2Se_4$ ω_0	$CdGa_2Se_4$ a	$CdGa_2Se_4$ b	$ZnGa_2Se_4$ ω_0	$ZnGa_2Se_4$ a	$ZnGa_2Se_4$ b
1	$E_{LO,TO}$	84	0.63	3.62	108	0.12	1.68	66	0.30	3.66	84	−0.14	2.72
2	$B_{LO,TO}$	87	0.88	−0.22	111	1.13	1.48	73	1.28	2.21	90	1.30	3.19
3	$E_{LO,TO}$	136	0.52	2.63	139	0.44	0.77	102	0.24	1.32	106	0.33	0.31
4 *a,b*	$B_{LO,TO}$	162, 168	−0.03, −0.02	0.38, 4.65	171, 175	0.56, 0.43	1.64, 0.08	121	0.28	0.95	126	0.50	1.61
5	$E_{LO,TO}$	242	6.54	8.55	264	5.69	8.37	176	5.73	14.56	180	3.10	6.10
6	$B_{LO,TO}$	261	2.07		279	6.38	11.16	194	4.81				
7 *a,b*	$B_{LO,TO}$	323	2.29					221, 226	2.43, 3.12	2.76, 6.17	234	1.83	1.91
8 *a,b*	$E_{LO,TO}$	323, 351	4.89, 4.40	8.07, 9.80	335	3.87	3.01	238, 245	4.41, 4.45	8.50, 8.78	243	4.34	5.60
9 *a,b*	E, B_{TO}	366, 367	3.49, 7.02	1.48, 18.5	361, 373	4.01, 5.42	4.39, 8.44	258	5.44	13.77			
10 *a,b*	E, B_{LO}	389, 394	5.71, 5.71	8.16, 6.93	396	4.68	5.00	275	4.90	6.23	285	3.40	4.25
	A^1	219	6.36	1.62	232	6.16	7.14	138	4.85	7.23	143	4.38	4.37
	A^2	311	4.72	5.73	321	4.46	5.89	185	3.56	6.45	[180]		
	A^3	362	3.66	5.96				207	2.74	2.71	209	2.70	2.49

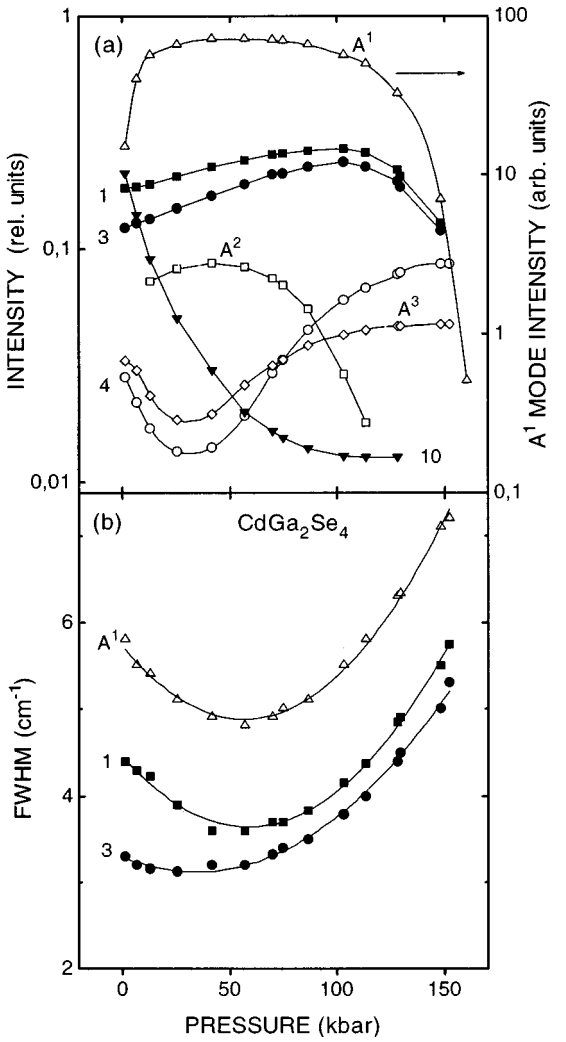

FIG. 5. (a) Right-hand side intensity axis: pressure dependence of the intensity of the A^1 mode for $CdGa_2Se_4$. Left-hand side intensity axis: intensities of other modes normalized to that of the A^1 mode. (b) FWHM of some modes for $CdGa_2Se_4$ at various pressures.

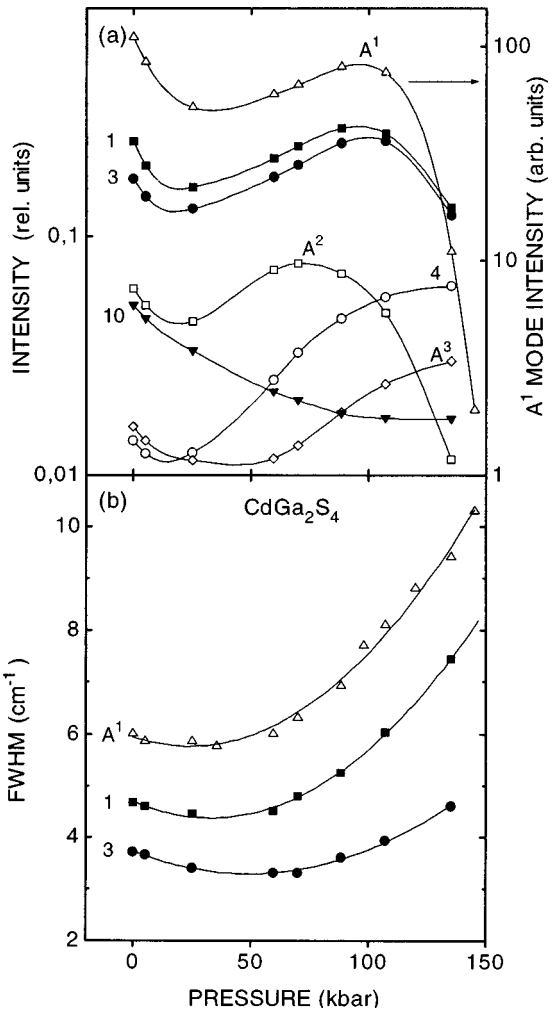

FIG. 6. Same as Fig. 5 for $CdGa_2S_4$.

7(a) illustrates the pressure dependence of the RS modes intensity for $ZnGa_2S_4$ crystals. As the pressure increases the intensity of all bands decreases (e.g., A^1 mode). At pressures above 160 kbar the intensity of the modes starts to decrease drastically and the RS signal disappears completely at pressures around 220 kbar. The intensity of the modes (except for the A^2 mode) slightly increases up to pressures of about 160 kbar when normalized to the intensity of the A^1 mode. The intensity of the A^2 mode decreases faster than that of the A^1 mode with increasing pressure. The FWHM of the modes exhibits two minima at pressures around 40 and 160 kbar, shown in Fig. 7(b).

The behavior of the RS modes with pressure in $ZnGa_2Se_4$ crystals is similar to that observed in $ZnGa_2S_4$. Figure 8 presents the pressure dependence of the A^1 mode intensity and the FWHM for the most intensive modes in $ZnGa_2Se_4$. The increase of RS signal at low pressures is caused, as in $CdGa_2Se_4$, by the resonance moving away from the laser line with pressure. The band gap of $ZnGa_2Se_4$ at room temperature and ambient pressure equals 2.58 eV. However, unlike $CdGa_2Se_4$, there is an extended exponential tail of electron states under the bottom of the conduction band, caused by the disorder in the cation sublattice.[1] This is the reason for the sharper increase in intensity than in $CdGa_2Se_4$ at low pressures. The intensity of the modes starts to decrease at pressures above 100 kbar and the RS signal disappears completely and irreversibly at pressures around 180 kbar. The first minimum in the FWHM pressure dependence seems to be centered at the ambient pressure, the second one being located near 105 kbar.

After releasing the pressure the RS signal in $CdGa_2Se_4$ and $ZnGa_2Se_4$ did not recover. In $CdGa_2S_4$ and $ZnGa_2S_4$ the Raman signal was found to recover only at pressures below 10 kbar. However, the recovered spectra were not similar to the initial ones, exhibiting well-defined features of amorphization (see Figs. 9 and 10). Such pressure-induced amorphization process has already been observed in IV and III-V tetrahedrally bonded materials,[33–35] as well as in the DC $ZnAl_{2(1-x)}Ga_{2x}S_4$ crystals and wurtzite-type $ZnAl_2S_4$.

It is to be noted that the decompressed compounds $CdGa_2S_4$ and $ZnGa_2S_4$ represent transparent crystallites. Apart from that, the intensity of the recovered RS signal for these materials is much lower than the initial one for noncompressed crystals. In our opinion, this indicates that the decompressed materials $ZnGa_2S_4$ and $CdGa_2S_4$ are only partially amorphous and consist mainly of a Raman-inactive high-pressure phase. Notice that the decompressed $CdGa_2Se_4$

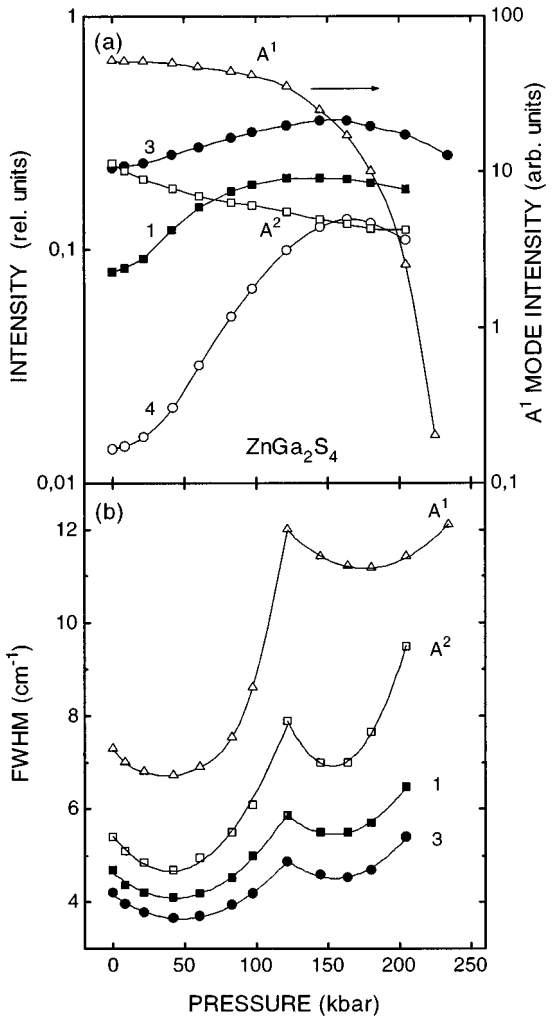

FIG. 7. Same as Fig. 5 for $ZnGa_2S_4$.

and $ZnGa_2Se_4$ are opaque crystals, whereas the initial crystals are of red color. One can conclude that the decompressed $ZnGa_2Se_4$ and $CdGa_2Se_4$ belong to the quenched high-pressure phase.

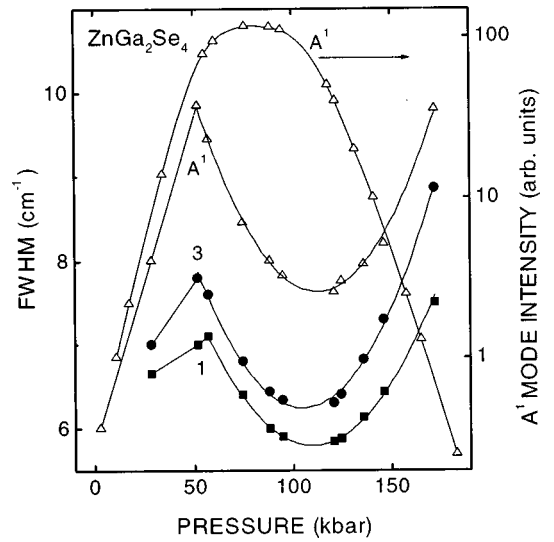

FIG. 8. Pressure dependence of the A^1 mode intensity and FWHM for the most intensive modes in $ZnGa_2Se_4$.

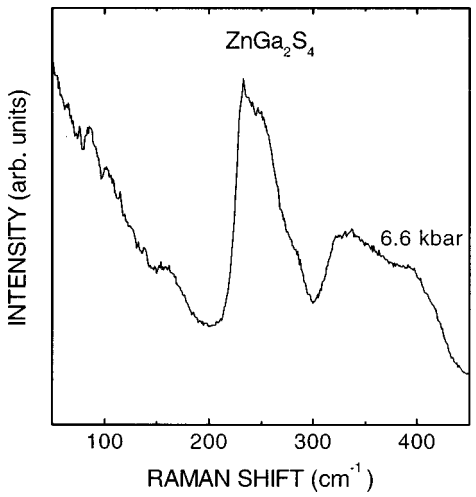

FIG. 9. Raman spectra of decompressed $ZnGa_2S_4$.

During the second compression of $CdGa_2S_4$ the intensity of the A^1 mode of the DC phase increases at intermediate pressure around 30 kbar; at the same time some other modes can be distinguished (see Fig. 10). One can conclude that the recrystallization of the DC phase occurs during the second compression. If the pressure is increased higher than 30 kbar the RS signal gradually disappears. However, the DC phase proves to be quenched when the pressure is released from 30 kbar.

IV. DISCUSSION

Essential changes in the RS spectrum of DC crystals begin at 55 kbar in $CdGa_2Se_4$ and 80 kbar in $CdGa_2S_4$. At these pressures one of the *A*-symmetry modes sharply decreases in intensity while their FWHM starts to increase with pressure. An analogous behavior has been observed in $CdAl_2S_4$ crystals of DC structure at $P>60$ kbar (see Ref. 9) and it was related to a transition from the DC structure to the cation-disordered phase, which has only two *A*-symmetry modes like the DF structure. The disorder in the cationic sublattice of $CdAl_2S_4$ occurs in two stages, as predicted earlier.[11] The

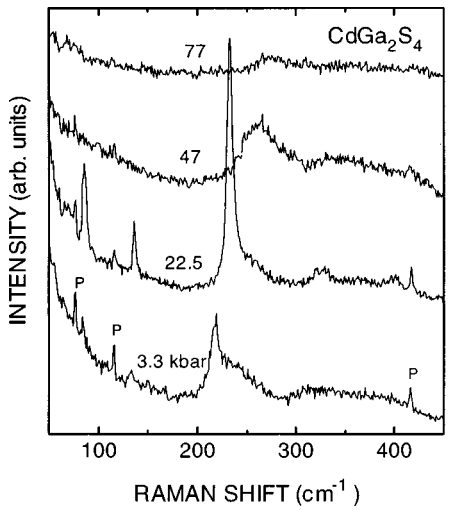

FIG. 10. Raman spectra of $CdGa_2S_4$ at various pressures during the second pressure cycle.

second stage of disorder in $CdAl_2S_4$ begins at about 100 kbar (Ref. 9). The sharp decrease of the ''breathing'' mode intensity is attributed to the involvement of stoichiometric vacancies in the disorder process that leads to the violation of the repetition law for the vacant sites. The mutual disorder of both types of cations and vacancies implies a complete disorder in the cation sublattice that is responsible for the formation of a disordered zinc-blendelike phase. As one can see from Figs. 5 and 6, the pressure of the second stage of disorder, indicated by the sharp decrease of A^1 mode, is about 110 kbar in $CdGa_2Se_4$ and 100 kbar in $CdGa_2S_4$.

As concerns the DF structure, it exhibits only two A-symmetry modes from the very beginning and no sharp decrease of the A^2 mode is expected. According to Fig. 7, a gradual decrease of A^2 mode intensity with pressure is characteristic of $ZnGa_2S_4$ crystals. Nevertheless, the two minima observed in the pressure dependence of the FWHM for $ZnGa_2S_4$ and $ZnGa_2Se_4$ crystals (see Figs. 7 and 8) reflect, in our opinion, two stages of disorder in the cation sublattice as well. The DF structure of $ZnGa_2S_4$ is characterized by partial cation disorder, Zn and Ga(1) being randomly distributed at $(4d)$ 0, $\frac{1}{2}$, $\frac{1}{4}$ sites, the Ga(2) being at the origin sites.[25] Thus, at a pressure of 40 kbar the Ga(2) atoms are involved in the first stage of disorder and the DF structure transforms from a partially cation disordered phase to a totally cation disordered one. $ZnGa_2Se_4$ is totally cation disordered already at ambient pressure, i.e., the first minimum of FWHM is at zero pressure. However, the stoichiometric vacancies are still not involved in the process of disorder. The vacancies are involved in the disorder process during the second stage, beginning at pressures 160 and 100 kbar for $ZnGa_2S_4$ and $ZnGa_2Se_4$, respectively. The occurrence of this stage is indicated by the second minimum in the pressure dependence of FWHM and by the sharp decrease of the mode's intensity at these pressures (see Figs. 7 and 8). As a result, a disordered zinc-blende-type phase is formed similar to the DC crystals.

An additional feature in favor of the first stage of disorder is the soft character of the lowest-energy E-symmetry mode. The frequency decrease of this mode with pressure reflects the initiation of the phase transition.[36] In order to appreciate more accurately the pressure value P_s at which the frequency of the lowest-energy E mode starts to decrease, we have plotted the pressure dependence of the frequency shift (Fig. 11). The above-mentioned P_s value equals 0, 36, 40, and 85 kbar for $ZnGa_2Se_4$, $ZnGa_2S_4$, $CdGa_2Se_4$, and $CdGa_2S_4$, respectively.

Earlier it was shown that the order-disorder transition with temperature can take place only in the chalcopyrites with axial ratio $c/a>1.95$ (Ref. 16). Compounds with $c/a<1.95$ remain in the ordered chalcopyrite structure all the way up to the melting point. Apart from that, the order-disorder behavior and the tetragonal distortion δ ($\delta=2-c/a$) of the chalcopyrite compounds ABC_2 can be described in terms of the difference in electronegativities $\Delta\chi_{AB}$ between the A-C and B-C bonds.[16] Chalcopyrites with $\Delta\chi_{AB}<0.09$ exhibit an order-disorder solid-state transition, whereas the chalcopyrites with $\Delta\chi_{AB}>0.09$ remain in the ordered chalcopyrite structure up to their melting point. The tetragonal distortion δ and the difference in electronegativities calculated as

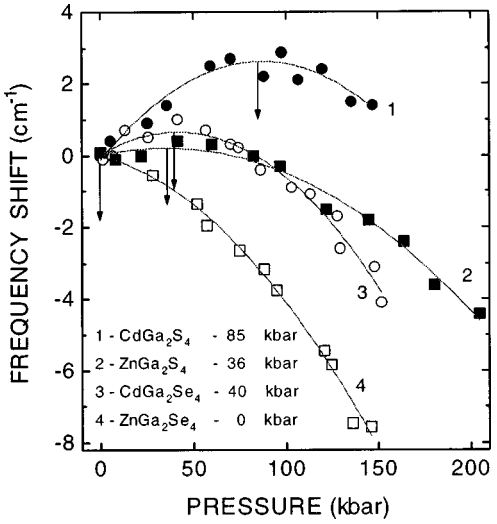

FIG. 11. Pressure dependence of the frequency shift for the lowest energy E-symmetry mode of AGa_2X_4 compounds. The arrows indicate the P_s values.

$$\Delta\chi_{AB}=\{r(A,B)/[r(C)-2dr_d(C)]\}\approx\{r(A,B)/r(C)\} \tag{1}$$

for the $A^{II}B_2^{III}C_4^{VI}$ materials under consideration are presented in Table II. As one can see from the table, the materials with $\Delta\chi_{AB}<0.09$ and $\delta<0.05$ ($ZnGa_2S_4$ and $ZnGa_2Se_4$) crystallize as DF whereas the compounds with $\Delta\chi_{AB}>0.09$ and $\delta>0.05$ ($CdGa_2S_4$ and $CdGa_2Se_4$) crystallize as DC.

On the other hand, the temperature-induced order-disorder transitions were recently investigated in $A^{II}B_2^{III}C_4^{VI}$ compounds.[20,37,38] When analyzing these data it was observed that the lower the δ the higher the temperature of the order-disorder transition. However, unlike chalcopyrites, in the DC $A^{II}B_2^{III}C_4^{VI}$ compounds the order-disorder transitions with temperature can occur in materials with $\delta>0.05$ as well. This different behavior can be explained by the presence of stoichiometric vacancies in the DC phase. Figure 12 presents the variation with the tetragonal distortion δ of the P_s pressure of the E mode (a) as well as the pressure of the first stage of order-disorder transition (b) determined from the pressure dependencies of mode intensities and FWHM, as mentioned above. As one can see from Fig. 12, a clear correlation exists between these pressures and δ in AB_2C_4 materials.

Some additional comments can be made concerning the behavior of the relative intensity of the two lowest E-symmetry modes in the DC crystals. Taking into account their similarity to the corresponding modes of zinc-blende

TABLE II. The tetragonal distortion δ and difference $\Delta\chi_{A,B}$ in electronegativities between the A-C and B-C bonds for the $A^{II}B_2^{III}C_4^{VI}$ materials.

Compound	$\Delta\chi_{AB}$	δ
$CdGa_2S_4$	0.124	0.17
$CdGa_2Se_4$	0.118	0.13
$ZnGa_2S_4$	0.042	0.04
$ZnGa_2Se_4$	0.040	0

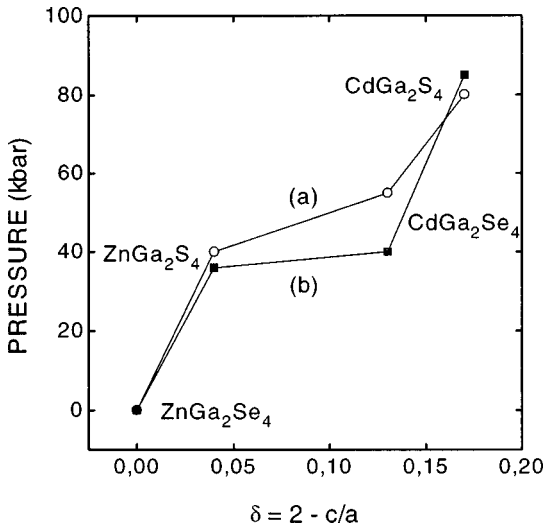

FIG. 12. Pressure value of the first stage of order-disorder transition in AGa_2X_4 compounds determined from the pressure dependence of mode intensities and FWHM (a), and from the point where the frequency of the lowest-energy E-symmetry mode starts to decrease (b).

(ZB) structure, one may conclude that modes 1 and 3 correspond to the W_4 and X_5 points of the ZB structure, respectively.[32] The increase of their intensity and linewidth (Figs. 5–8) after the first order-disorder phase transition can be explained by large anharmonic contributions to the lattice vibrations. An analogous effect has been observed in the overtone transverse-acoustical 2TA of ZB in ZnSe (Ref. 39) and in the $G_5(X_5)$ and $G_5(W_4)$ modes in a $CuGaS_2$ chalcopyrite compound.[5] In both cases this fact was accounted for by a redistribution, under pressure, of the density of the electrons responsible for the bond-restoring forces; this redistribution, in turn, leads to an increase of the electron-phonon interaction, as the transition to the high-pressure phase is approached.

Finally, we will discuss the disappearance of RS signals at high pressures. By analogy to the adamantine structure compounds, we assume that this effect is caused by a phase transition to a sixfold-coordinated rocksalt-type structure.

The microscopic dielectric theory of Phillips and Van-Vechten[40] provides a basis for understanding the structural trends of semiconductors. In Table III we summarize the homopolar energy gap E_h and ionic energy C for most of the $A^{\mathrm{I}}B^{\mathrm{III}}C_2^{\mathrm{VI}}$ CP compounds (according to Refs. 41 and 42) as well as for $A^{\mathrm{II}}B_2^{\mathrm{III}}C_4^{\mathrm{VI}}$ DC compounds. The values of E_h and C for $A^{\mathrm{II}}B_2^{\mathrm{III}}C_4^{\mathrm{VI}}$ compounds were calculated from

$$E_h=(E_{h,AC}+2E_{h,BC})/3 \tag{2}$$

and

$$C=(C_{AC}+2C_{BC})/3, \tag{3}$$

while the average energy gaps from

$$E_g^2=E_h^2+C^2. \tag{4}$$

Figure 13 shows a phase diagram containing most of the $A^{\mathrm{I}}B^{\mathrm{III}}C_2^{\mathrm{VI}}$ with CP and $A^{\mathrm{II}}B_2^{\mathrm{III}}C_4^{\mathrm{VI}}$ with DC structure at ambient pressure. The homopolar energy gap E_h and the ionic energy gap C are plotted along the horizontal and vertical axes, respectively. A circle centered at the origin is drawn to separate the two high-pressure phases according to the theory of Phillips and Van-Vechten. We see that all compounds involved fall outside this circle, indicating that a phase transition to the rocksalt-type structure is expected under pressure. It is to be noted that the high-pressure rocksalt-structure phase has been confirmed by x-ray analysis for most of the $A^{\mathrm{I}}B^{\mathrm{III}}C_2^{\mathrm{VI}}$ compounds.

TABLE III. The homopolar (E_h), ionic (C), and average (E_g) energy gap for ABC_2 and AB_2C_4 compounds. All energies are in eV units.

Compound	E_h	C	E_g
ABC_2			
$CuAlS_2$	5.078	8.161	9.612
$CuAlSe_2$	4.490	7.300	8.570
$CuAlTe_2$	3.789	6.257	7.315
$CuGaS_2$	4.795	7.679	9.053
$CuGaSe_2$	4.254	6.955	8.153
$CuGaTe_2$	3.713	6.141	7.176
$CuInS_2$	4.207	6.711	7.921
$CuInSe_2$	4.133	6.900	8.043
$CuInTe_2$	3.463	5.298	6.329
$AgAlS_2$	4.605	7.630	8.912
$AgAlSe_2$	4.118	6.887	8.024
$AgAlTe_2$	3.469	5.970	6.905
$AgGaS_2$	4.529	7.495	8.757
$AgGaSe_2$	4.050	6.820	7.932
$AgGaTe_2$	3.447	5.983	6.905
$AgInS_2$	4.138	7.222	8.323
$AgInSe_2$	3.705	6.520	7.499
$AgInTe_2$	3.171	5.656	6.484
AB_2C_4			
$CdAl_2S_4$	4.679	5.831	7.476
$CdGa_2S_4$	4.638	5.789	7.420
$CdGa_2Se_4$	5.071	6.015	7.867
$ZnGa_2S_4$	4.177	5.269	6.720
$ZnGa_2Se_4$	4.477	5.400	7.015

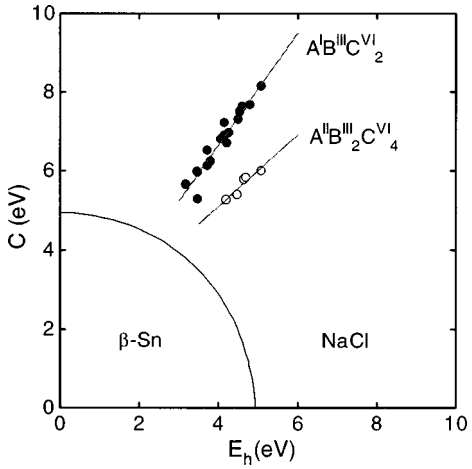

FIG. 13. Phase diagram for $A^{\mathrm{I}}B^{\mathrm{III}}C_2^{\mathrm{VI}}$ and $A^{\mathrm{II}}B_2^{\mathrm{III}}C_4^{\mathrm{VI}}$ compounds at ambient pressure. The data are presented in Table III. Solid lines are only to assist the eye.

TABLE IV. Bond ionicity ($f^i_{AC,BC}$), bond length ($d_{AC,BC}$), crystal ionicity (f^i), average bond length (d) (Refs. 40–43), and the experimental transition pressure to the rocksalt-type structure for ABC_2 and AB_2C_4 compounds.

Compound	f^i_{AC}	f^i_{BC}	f^i	d_{AC} (Å)	d_{BC} (Å)	d (Å)	P_{NaCl} (kbar)
ABC_2							
$CuAlS_2$	0.813	0.561	0.687	2.374	2.219	2.297	150
$CuGaS_2$	0.816	0.561	0.689	2.340	2.255	2.298	165
$CuGaSe_2$	0.825	0.567	0.696	2.395	2.410	2.403	136
$CuInS_2$	0.808	0.569	0.689	2.310	2.490	2.400	96
$CuInSe_2$	0.817	0.572	0.695	2.440	2.580	2.510	71
$AgGaS_2$	0.849	0.559	0.704	2.575	2.255	2.415	150
$AgGaSe_2$	0.851	0.566	0.709	2.601	2.416	2.509	83
$AgInSe_2$	0.850	0.573	0.712	2.600	2.625	2.613	25
AB_2C_4							
$CdAl_2S_4$	0.685	0.561	0.602	2.532	2.255 2.249	2.395	140
$CdGa_2S_4$	0.685	0.561	0.602	2.435	2.372 2.298	2.368	150
$CdGa_2Se_4$	0.699	0.567	0.611	2.637	2.411 2.416	2.488	150
$ZnGa_2S_4$	0.623	0.561	0.582	2.303	2.328 2.278	2.201	220
$ZnGa_2Se_4$	0.630	0.567	0.588	2.455	2.416 2.416	2.429	180

Chelikowsky has used a combination of pseudopotential total-energy method with an empirical ionicity scale to predict phase transitions as a function of pressure for all diamond and zinc-blende semiconductors of the form $A^N B^{8-N}$, where A and B are simple metals or metalloids and N is the number of valence electrons for species A.[43,44] Two parameters enter into his discussion, the crystal ionicity from the dielectric theory and the equilibrium crystal volume. Since the phase transition to the rocksalt structure under pressure in $A^{\mathrm{II}}B_2^{\mathrm{III}}C_4^{\mathrm{VI}}$ DC compounds takes place through a disordered ZB-like structure, it is reasonable to require whether the above theory applies to the CP and DC compounds. For this purpose we present in Table IV the ionicities and bond lengths for $A^{\mathrm{I}}B^{\mathrm{III}}C_2^{\mathrm{VI}}$ and $A^{\mathrm{II}}B_2^{\mathrm{III}}C_4^{\mathrm{VI}}$ compounds along with experimental values of phase transition pressures to the rocksalt structure. The ionicities of A^{I}-C^{VI} and B^{III}-C^{VI} bonds were taken from Ref. 41. The ionicities of A^{II}-C^{VI} bonds are from Ref. 40. The bond lengths d_{AC} and d_{BC} correspond to those presented in Refs. 45 and 46. In previous studies of the trends in the material properties of ABC_2 compounds it has been shown that the arithmetic means

$$f_i=(f_{i\,AC}+f_{i\,BC})/2 \tag{5a}$$

of the ionicities $f_{i\,AC}$ and $f_{i\,BC}$ of the individual bonds A^{I}-C^{VI} and B^{III}-C^{VI} give an appropriate value for the average-bond ionicity of the ABC_2 compounds.[41] Taking this into account we have calculated the average-bond ionicity of the AB_2C_4 compounds as

$$f_i=(f_{i\,AC}+2\,f_{i\,BC})/3. \tag{5b}$$

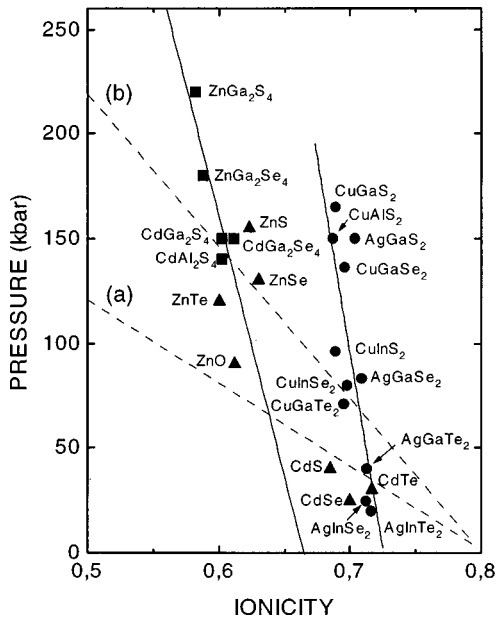

FIG. 14. Critical pressure for transformation from the fourfold-coordinated structure to the sixfold-coordinated one, as a function of ionicity for $A^{\mathrm{II}}B^{\mathrm{VI}}$, $A^{\mathrm{I}}B^{\mathrm{III}}C_2^{\mathrm{VI}}$, and $A^{\mathrm{II}}B_2^{\mathrm{III}}C_4^{\mathrm{VI}}$ compounds. The dashed lines are the results of calculation following (a) the Chelikowsky (Ref. 44), and (b) the Christensen (Ref. 47) model. Solid lines are the linear least-squares fits of the experimental data.

The bond lengths in $A^{\mathrm{I}}B^{\mathrm{III}}C_2^{\mathrm{VI}}$ compounds were calculated as

$$d=(d_{AC}+d_{BC})/2, \tag{6a}$$

while in $A^{\mathrm{II}}B_2^{\mathrm{III}}C_4^{\mathrm{VI}}$ compounds as

$$d=(d_{AC}+2d_{BC})/3. \tag{6b}$$

Figure 14 illustrates the transition pressure for the transformation from the fourfold-coordinated structure to the sixfold-coordinated one, as a function of ionicity, for $A^{\mathrm{II}}B^{\mathrm{VI}}$, $A^{\mathrm{I}}B^{\mathrm{III}}C_2^{\mathrm{VI}}$, and $A^{\mathrm{II}}B_2^{\mathrm{III}}C_4^{\mathrm{VI}}$ compounds. The dashed lines in the figure are the result of calculations according to the model of Chelikowsy[44] and the frozen-potential model of Christensen, Satpathy, and Pawlowska.[47] The solid lines are the linear least-squares fits of the experimental data for $A^{\mathrm{I}}B^{\mathrm{III}}C_2^{\mathrm{VI}}$ and $A^{\mathrm{II}}B_2^{\mathrm{III}}C_4^{\mathrm{VI}}$ compounds. One can observe that Chelikowsky's theoretical results fit very well the experimental data for the $A^{\mathrm{II}}B^{\mathrm{VI}}$ materials with high ionicity. [The opposite is true for the theoretical results of Christensen, Satpathy, and Pawloska.] Specifically, it was found that MgS and MgSe fall on the transition boundary of zinc-blende and rocksalt structures, the predicted critical ionicity being consistent with the Phillips value. [Chelikowsky has found $f_1^c=0.80$, in close agreement with the Phillips value $f_1^c=0.795$.] For the materials with low ionicity the agreement with experiment is only qualitative. Nevertheless, the theoretical approach predicts a difference between the Zn and Cd salts. Namely, the Zn salts should possess a higher transition pressure from ZB to rocksalt structure than the Cd salts. This general trend is confirmed by experiment. Furthermore, we observe that this trend is valid for our $A^{\mathrm{II}}B_2^{\mathrm{III}}C_4^{\mathrm{VI}}$ compounds as well.

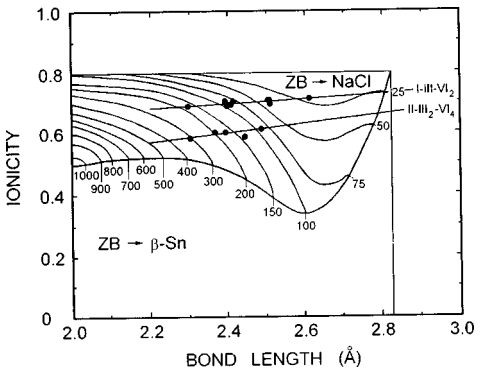

FIG. 15. Same as Fig. 3 from Ref. 44 with experimental data summarized in Table IV for $A^{I}B^{III}C_2^{VI}$ and $A^{II}B_2^{III}C_4^{VI}$ compounds. Solid lines are only to assist the eye.

As concerns $A^{I}B^{III}C_2^{VI}$ CP and $A^{II}B_2^{III}C_4^{VI}$ DC compounds, we observe that the experimental data are very well approximated by the linear fits (which, however, differ substantially from those of Chelikowsky and Christensen, Satpathy, and Pawloska).

Another essential output from Chelikowsky's model is the possibility to predict the transition pressure and the high-pressure structure (rocksalt or β-Sn). In Fig. 15 we have included the experimental data for $A^{I}B^{III}C_2^{VI}$ CP and $A^{II}B_2^{III}C_4^{VI}$ DC compounds in high-pressure domains for diamond and ZB semiconductors calculated by Chelikowsky.[44] The transitions from the ZB to white tin (ZB–β-Sn) and from ZB to rocksalt (ZB–NaCl) are indicated in an ''ionicity-bond-length'' space. Above the critical ionicity of 0.79, the ZB structures are not stable at normal pressure. Also, for bond lengths greater than 2.8 Å no ZB structures exist. The theory is not applicable to compounds with bond length less than ~2.3 Å. One can see that all $A^{I}B^{III}C_2^{VI}$ CP and $A^{II}B_2^{III}C_4^{VI}$ DC compounds lay in the ZB-NaCl domain. Thus, a transition to the rocksalt structure is expected.

Figure 15 also displays a contour plot of transition pressures to the rocksalt phase predicted by Chelikowsky's model. Table V presents the comparison between the experimental and the predicted high-pressure forms and transition pressure for $A^{I}B^{III}C_2^{VI}$ and $A^{II}B_2^{III}C_4^{VI}$ compounds. We can conclude that the agreement between theory and experiment is satisfactory. However, the predicted transition pressures for the sulfides are overestimated, while for selenides they are underestimated. One can notice the same tendency for ZB $A^{II}B^{VI}$ compounds when analyzing the data presented by Chelikowsky.[44] This behavior can be accounted for by the fact that the calculations do not include explicit treatment of *d*-orbital effects.

In short, the first stage of order-disorder phase transition in AB_2C_4 compounds is determined by the tetragonal distortion. The final phase transition from a fourfold-coordinated structure to a sixfold-coordinated one is influenced by ionicity. Concerning the intermediate second stage of order-disorder transition in AB_2C_4 compounds, there is no evident influence of the same parameters on the transition pressure, the latter being nearly the same for all materials.

Finally we discuss the structure of the materials after pressure release. It was shown recently on the basis of a configuration-coordinate model,[33,34] that the structure of decompressed tetrahedrally bonded materials is determined by the pressure dependence of the height of potential barrier between the high- and low-pressure phases on the one hand, and that between high-pressure and amorphous phase on the other. Figure 16 illustrates the schematic diagram for the height of the potential barriers between the high-pressure (in our case of rocksalt-type) phase and the amorphous phase $U_{\text{NaCL-AM}}$ and between the high- and low-pressure phases $U_{\text{NaCl-DC}}$, as a function of pressure for tetrahedrally coordinated AB_2C_4 compounds. P_i represents the pressure where $U_{\text{NaCL-AM}}$ equals $U_{\text{NaCl-DC}}$. The metastable high-pressure phase is quenched when the thermal energy is lower than the height of both potential barriers. For binary $A^{II}B^{VI}$ and $A^{III}B^{V}$ tetrahedrally bonded materials this occurs only at low temperatures, while in AB_2C_4 materials it occurs even at room temperature (see path 1 in Fig. 16). With decreasing

TABLE V. Comparison between theoretically predicted transition pressures to the rocksalt-type structure and their experimental values for ABC_2 and AB_2C_4 compounds.

Compound	Theor.	Expt.
ABC_2		
$CuAlS_2$	170	150
$CuGaS_2$	170	165
$CuGaSe_2$	80	136
$CuInS_2$	95	96
$CuInSe_2$	37	71
$AgGaS_2$	80	150
$AgGaSe_2$	40	83
$AgInSe_2$	24	25
AB_2C_4		
$CdAl_2S_4$	150	140
$CdGa_2S_4$	200	150
$CdGa_2Se_4$	90	150
$ZnGa_2S_4$	300	220
$ZnGa_2Se_4$	130	180

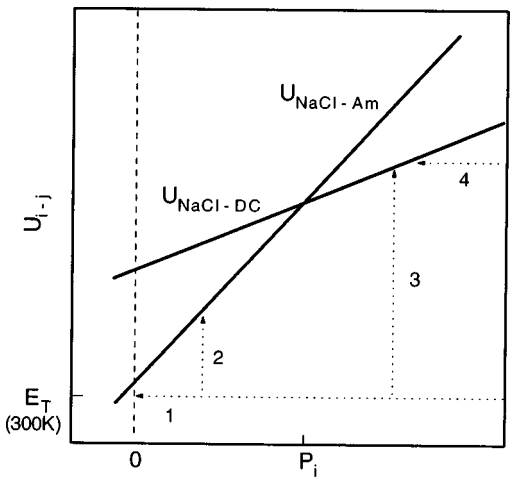

FIG. 16. Schematic diagram for the height of the potential barrier between high-pressure phase and amorphous phase ($U_{\text{NaCl-AM}}$) and between high-pressure and low-pressure phases ($U_{\text{NaCl-DC}}$), as a function of pressure for the $A^{II}B_2^{III}C_4^{VI}$ compounds.

pressure, the high-pressure phase transforms to the phase with the lowest possible potential barrier for a given thermal energy.

It was shown[34,35] that the pressure dependence of the potential barrier between high- and low-pressure phase $U_{\text{HP-LP}}$ is a function of ionicity. The ionic character of $A^{\text{II}}B^{\text{VI}}$ and some $A^{\text{III}}B^{\text{V}}$ compounds should lower $U_{\text{HP-LP}}$. In CdTe, for example, the large ionicity in the bonding nature lowers $U_{\text{HP-LP}}$ to such extent, that path 4 in Fig. 16 takes place at room temperature and the high-pressure phase returns to the initial ZB structure with pressure release. The ionicity of $A^{\text{II}}B_2^{\text{III}}C_4^{\text{VI}}$ materials, according to Fig. 14, is lower than that of $A^{\text{II}}B^{\text{VI}}$ materials; as a consequence, $U_{\text{NaCl-DC}}$ is higher. Therefore, at room temperature the phase transition is irreversible. In order to have reversible phase transition (following path 4) in AB_2C_4 materials it is necessary to release the pressure at temperatures higher than the room temperature. Another peculiarity of tetrahedrally bonded AB_2C_4 materials is that the potential barrier between the high-pressure phase and the amorphous phase $U_{\text{NaCl-AM}}$ is higher than in $A^{\text{II}}B^{\text{VI}}$ and $A^{\text{III}}B^{\text{V}}$ materials. This is the reason why no amorphization occurs with releasing pressure at room temperature in $ZnGa_2Se_4$ and $CdGa_2Se_4$. In materials containing sulfur the $U_{\text{NaCL-AM}}$ is somewhat lower and partial amorphization occurs in decompressed $ZnGa_2S_4$ and $CdGa_2S_4$ (path 1 in Fig. 16). In order to obtain total amorphization it is necessary to increase the temperature at pressures lower than P_i (path 2 in Fig. 16). With increasing temperature, the quenched metastable high-pressure phase transforms to the phase with the lowest possible potential barrier. If the temperature is increased at pressures higher than P_i the quenched phase will transform to the DC structure (path 3 in Fig. 16).

As concerns recrystallization occurring in $CdGa_2S_4$ during the second compression, an analogous process was observed in GaSb at pressures around 40 kbar (see Ref. 35). It should be noted that crystallization under pressure is a peculiarity of pressure-induced amorphization and as such does not characterize as-grown amorphous materials.[35] A simple explanation is that the structural disorder is large in pressure-amorphized materials.

V. CONCLUSION

An order-disorder phase transition takes place in the cation sublattice of tetrahedrally bonded $A^{\text{II}}Ga_2X_4^{\text{VI}}$ compounds under hydrostatic pressure. This transition occurs in two stages following earlier predictions by Bernard and Zunger.[11] The compounds with $A=\text{Cd}$ belong to the DC structure characterized by totally ordered cations and stoichiometric vacancies. In the first stage of order-disorder transition, disordering among Cd and Ga cations takes place. The compounds with $A=\text{Zn}$ belong to DF structure with partial disorder in the cation sublattice. In this case, in the first stage of transition it is the ordered Ga atoms at the origin sites that are involved in the disordering process and Zn and Ga cations become totally disordered. In the second stage the stoichiometric vacancies are involved in the process of disorder in both DC and DF structures. The mutual disorder of both types of cations and vacancies leads to the formation of the disordered ZB-like phase. The first stage of order-disorder phase transition is determined by the tetragonal distortion of initial crystals. The irreversible disappearance of RS signal at higher pressures is supposed to be caused by the phase transition from the adamantine structure to a Raman-inactive rocksalt-type structure. Such a transition is influenced by the bond ionicity and bond length. After releasing the pressure at room temperature in Se-containing AGa_2X_4 compounds, the high-pressure rocksalt-type structure is quenched. On the other hand, decompression of S-containing compounds leads to partial amorphization. These results are discussed on the basis of a configuration-coordinate model taking into account the pressure dependence of potential barriers for the phase transition.

ACKNOWLEDGMENTS

This work was partially supported by NTUA and the General Secretariat for Research and Technology, Greece.

[1] A. N. Georgobiani, S. I. Radautsan, and I. M. Tiginyanu, Fiz. Tekh. Poluprovodn. **19**, 193 (1985) [Sov. Phys. Semicond. **19**, 121 (1985)].
[2] S. I. Radautsan and I. M. Tiginyanu, Jpn. J. Appl. Phys., Suppl. **32-3**, 5 (1993).
[3] M. I. McMahon and R. J. Nelmes, J. Phys. Chem. Solids **56**, 485 (1995).
[4] R. J. Nelmes, M. I. McMahon, N. G. Wright, and D. R. Allan, J. Phys. Chem. Solids **56**, 545 (1995).
[5] J. Gonzales, B. J. Fernandez, J. M. Besson, M. Gauthier, and A. Pollian, Phys. Rev. B **46**, 15 092 (1992).
[6] T. Tinoco, A. Polian, J. P. Itie, E. Moya, and J. Gonzalez, J. Phys. Chem. Solids **56**, 481 (1995).
[7] J. Gonzalez, E. Colderon, T. Tinico, J. P. Itie, A. Polian, and E. Moya, J. Phys. Chem. Solids **56**, 507 (1995).
[8] E. Anastassakis, Y. S. Raptis, S. H. Ando, T. Irie, V. V. Ursaki, I. M. Tiginyanu, S. I. Radautsan, and I. I. Burlakov, Cryst. Res. Technol. **31**, S1, 365 (1996).
[9] I. I. Burlakov, Y. S. Raptis, V. V. Ursaki, E. Anastassakis, and I. M. Tiginyanu, Solid State Commun. **101**, 377 (1997).
[10] I. M. Tiginyanu, Y. S. Raptis, V. V. Ursaki, E. Anastassakis, and I. I. Burlakov, Cryst. Res. Technol. **31**, S2, 777 (1996).
[11] J. E. Bernard and A. Zunger, Phys. Rev. B **37**, 6835 (1988).
[12] K.-J. Range, W. Becker, and A. Weiss, Z. Naturforsch. B **23**, 1009 (1984).
[13] S. B. Bonsall and F. A. Hummel, J. Solid State Chem. **25**, 379 (1978).
[14] H. J. Berthold and K. Köhler, Z. Anorg. Allg. Chem. **475**, 45 (1981).
[15] M. E. Hills, D. C. Harris, and C. K. Lowe-Ma, J. Phys. Chem. Solids **48**, 501 (1987).
[16] J. J. M. Binsma, L. J. Giling, and J. Bloem, Phys. Status Solidi A **63**, 595 (1981).
[17] A. Zunger, Appl. Phys. Lett. **50**, 164 (1987).
[18] C. Rincon, Solid State Commun. **64**, 663 (1987).

[19] A. Miller, A. MacKinnon, and D. Weaire, Solid State Phys. **36**, 119 (1981).
[20] I. M. Tiginyanu, V. V. Ursaki, and V. N. Fulga, Fiz. Tekh. Poluprovodn. **237**, 821 (1977) [Sov. Phys. Semicond. **23**, 1069 (1989)].
[21] G. F. Mocharnyuk, T. I. Babyuk, O. P. Derid, L. S. Lazarenko, M. M. Markus, and S. I. Radautsan, Sov. Phys. Dokl. **22**, 749 (1977).
[22] L. Gastaldi, M. G. Simeone, and S. Viticali, Solid State Commun. **55**, 605 (1985).
[23] H. Haeuseler, J. Solid State Chem. **26**, 367 (1978).
[24] V. Framer, B. Frick, and D. Siebert, Z. Kristallogr. **165**, 151 (1983).
[25] V. Framer, B. Frick, and S. Febbraro, Z. Kristallogr. **169**, 283 (1984).
[26] G. B. Carpenter, P. Wu, Y.-M. Gao, and A. Wold, Mater. Res. Bull. **24**, 1077 (1989).
[27] P. P. Lottici and C. Razzetti, Solid State Commun. **46**, 681 (1983).
[28] I. M. Tiginyanu, P. P. Lottici, C. Razzetti, and S. Gennarri, Jpn. J. Appl. Phys., Suppl. **32-3**, 561 (1993).
[29] A. MacKinnon, J. Phys. C **12**, L655 (1979).
[30] A. Miller, D. J. Lockwood, A. MacKinnon, and D. Weaire, J. Phys. C **9**, 2997 (1976).
[31] C. Razzetti and P. P. Lottici, Jpn. J. Appl. Phys., Suppl. **32-3**, 431 (1993).
[32] Y. Maeyama, Y. Uchihashi, H. Kasahara, K. Yamamoto, and K. Abe, Jpn. J. Appl. Phys., Suppl. **22-3**, 193 (1983).
[33] M. Imai, K. Yaoita, Y. Katoyama, J.-Q. Chen, and K. Tsuji, J. Non-Cryst. Solids **150**, 49 (1992).
[34] K. Tsuji, Y. Katayama, N. Koyama, Y. Yamamoto, J.-Q. Chen, and M. Imai, J. Non-Cryst. Solids **156-158**, 540 (1993).
[35] K. Tsuji, Y. Katayama, Y. Yamamoto, H. Kanda, and H. Nosaka, J. Phys. Chem. Solids **56**, 559 (1995).
[36] E. Anastassakis, A. Pinczuk, E. Burstein, F. H. Pollack, and M. Cardona, Solid State Commun. **8**, 133 (1970).
[37] M. Dietrich, M. Unterricker, M. Deicher, A. Burchard, R. Magerle, W. Pfeiffer, D. Forkel-Wirth, I. M. Tiginyanu, and N. A. Moldovyan, Cryst. Res. Technol. **31**, 853 (1996).
[38] M. Dietrich, M. Unterricker, M. Deicher, A. Burchard, R. Magerle, W. Pfeiffer, D. Forkel-Wirth, I. M. Tiginyanu, and N. A. Moldovyan, Hyperfine Interact. **1**, 242 (1996).
[39] G. Weill, J. C. Chervin, and J. M. Besson, High Press. Res. **7**, 105 (1991).
[40] J. C. Phillips, *Bonds and Bands in Semiconductors* (Academic, New York, 1973).
[41] H. Neumann, Cryst. Res. Technol. **18**, 1391 (1983).
[42] V. Kumar, J. Phys. Chem. Solids **48**, 827 (1987).
[43] J. K. Chelikowsky and J. K. Burdett, Phys. Rev. Lett. **56**, 961 (1986).
[44] J. K. Chelikowsky, Phys. Rev. B **35**, 1174 (1987).
[45] H. Neumann, Cryst. Res. Technol. **26**, 1001 (1991).
[46] J. F. Jeffe and A. Zunger, Phys. Rev. B **29**, 1882 (1984) (see Table V, p. 1903).
[47] N. E. Christensen, S. Satpathy, and Z. Pawlowska, Phys. Rev. B **36**, 1032 (1987).